MIT Libraries | DSpace@MIT

MIT Open Access Articles

Optimal kinematics and morphologies for spermatozoa

The MIT Faculty has made this article openly available. ***Please share*** how this access benefits you. Your story matters.

Citation: Tam, Daniel, and A. Hosoi. "Optimal Kinematics and Morphologies for Spermatozoa." Physical Review E 83.4 (2011) ©2011 American Physical Society

As Published: http://dx.doi.org/10.1103/PhysRevE.83.045303

Publisher: American Physical Society

Persistent URL: http://hdl.handle.net/1721.1/65409

Version: Final published version: final published article, as it appeared in a journal, conference proceedings, or other formally published context

Terms of Use: Article is made available in accordance with the publisher's policy and may be subject to US copyright law. Please refer to the publisher's site for terms of use.

Massachusetts Institute of Technology

PHYSICAL REVIEW E **83**, 045303(R) (2011)

Optimal kinematics and morphologies for spermatozoa

Daniel Tam[1,*] and A. E. Hosoi[2]

[1]*Department of Mathematics, Massachusetts Institute of Technology, Cambridge, Massachusetts 02139, USA*

[2]*Department of Mechanical Engineering, Massachusetts Institute of Technology, Cambridge, Massachusetts 02139, USA*

(Received 24 August 2010; revised manuscript received 24 January 2011; published 22 April 2011)

We investigate the role of hydrodynamics in the evolution of the morphology and the selection of kinematics in simple uniflagellated microorganisms. We find that the most efficient swimming strategies are characterized by symmetrical, nonsinusoidal bending waves propagating from the base of the head to the tip of the tail. In addition, we show that the ideal tail-to-head length ratio for such a swimmer is $\approx$12 and that this predicted ratio is consistent with data collected from over 400 species of mammalian sperm.

DOI: 10.1103/PhysRevE.83.045303 PACS number(s): 47.63.Gd, 47.63.mf, 87.19.ru

It has been asserted that amidst "... increasing calls for biology to be predictive... [O]ptimization is the only approach biology has for making predictions from first principles" [1]. While this may indeed be the case, computing optima in biology is a nontrivial exercise, owing to the inherent complexity of biological systems. Even when sensible models can be constructed from first principles, the parameter space is vast. Hence there are relatively few examples in which biological data can be meaningfully compared with computed optimal solutions. Here we address these challenges by studying the swimming gaits of a highly specialized cell with a well-defined objective function: the sperm cell. The spermatozoon represents one of the simplest biological systems to exhibit locomotion. They are propelled by a beating, tail-like structure known as the eukaryotic flagellum [2] and their sole function is to transport genetic material to the ovum. The high levels of competition experienced by these cells suggest that they are well-adapted to fast and efficient locomotion at micron scales. Hence we considered a simple model problem: the optimization of swimming gaits and geometries of uniflagellated swimmers. Although solutions to this problem lie in a vast optimization space, we find well-defined optimal solutions that are in remarkable agreement with biological observations.

Studies on the hydrodynamics of flagellar propulsion were pioneered by Hancock [3] and later extended to investigate the efficiency of swimming stroke patterns for flagellated microorganisms. However, these early studies only considered prescribed kinematics [4,5], which consisted of traveling waves. More recent work has demonstrated the existence of optimal swimming strokes for a discretized swimming flagellum: the three-link swimmer [6]. In addition, many swimming mechanisms, which do not involve the deformation of flagella, have been discussed in the literature (see [7] and references therein).

The model uniflagellated swimmer in this study consists of a rigid spherical head of diameter D with a single flagellum of length L and radius r, swimming by itself in an infinite surrounding fluid of density ρ, which we assume to be Newtonian with dynamic viscosity μ. While this Newtonian assumption is valid for species with external fertilization, spermatozoa of species with internal fertilization, particularly mammals, may be subject to a viscoelastic environment such as cervical mucus in the cervical canal. It is noteworthy that this mucus is present in a small—albeit very important—part of the female reproductive tract, and during fertile periods it becomes increasingly hydrated, reducing the non-Newtonian characteristics and facilitating sperm penetrability [8]. Hence, as a first-order approximation, we model the surrounding fluid as Newtonian.

The swimmer translates by performing a "stroke" (i.e., periodic deformation) at a frequency f corresponding to a stroke period of $\tau = 1/f$ [see Fig. 1(a)]. Via dimensional analysis, one can deduce that the system involves three dimensionless parameters: the Reynolds number $\mathrm{Re} = \rho D^2 f/\mu$, the inverse slenderness of the tail $\kappa = L/r$, and the tail-to-head length ratio $\eta = L/D$. For spermatozoa in water, the Reynolds number is small ($\mathrm{Re} \sim 10^{-3}$) and can be neglected. Hence the dynamics are governed by Stokes equations

$$\nabla \cdot \boldsymbol{u} = \mathbf{0}, \quad -\nabla p + \mu \nabla^2 \boldsymbol{u} = \mathbf{0}, \tag{1}$$

where p is the pressure field and $\boldsymbol{u}$ is the incompressible velocity field.

We define the swimming efficiency $\mathcal{E}$ associated with a given stroke as

$$\mathcal{E} = \frac{\alpha U_0^2}{\phi}. \tag{2}$$

Here the numerator corresponds to the power required to translate the head alone (i.e., the "payload" of genetic material) at an average speed U_0, where $\alpha = 3\pi\mu D$ is the drag coefficient of the spherical head. The denominator ϕ represents the average mechanical power dissipated through viscosity during one stroke:

$$\phi = \left\langle \int\int_{\Sigma} (\boldsymbol{\sigma} \cdot \boldsymbol{n}) \cdot \boldsymbol{U} \, d\Sigma \right\rangle, \tag{3}$$

where Σ is the surface of the swimmer, $\boldsymbol{\sigma}$ is the hydrodynamic stress tensor, $\boldsymbol{n}$ is the unit normal vector to the surface, and $\boldsymbol{U}$ is the velocity at the surface of the swimmer. Angular brackets indicate a time average over one stroke period. The swimming efficiency, $\mathcal{E}$, can thus be interpreted as the fraction of the total energy expense effectively used to generate translation. Note that, because time can be scaled out of the Stokes equations, the efficiency $\mathcal{E}$ is a direct measure of the effectiveness of

*dan_tam@math.mit.edu

 ©2011 American Physical Society

the kinematics, in the sense of *both* efficiency (minimizing energy expenditure for a given swimming speed) and speed (maximizing velocity for a given energy budget).

All possible periodic strokes are defined by a local curvature function $\gamma(s,t)$, where the coordinate $s = 0,\ldots,L$ denotes the arc length and $t = 0,\ldots,\tau$ is time. We limited our investigation to planar deformations, which are both biologically relevant and sufficiently simple to be suited to numerical optimization. For a given $\gamma(s,t)$, the motion of the swimmer can be computed by solving for the flow induced by the deformation of the flagellum and enforcing force and torque equilibrium on the swimmer. These governing equations are solved using slender-body theory for the hydrodynamics around the flagellum, in which fundamental solutions to the Stokes equations are distributed along the centerline of the swimmer such that the no-slip boundary condition is satisfied to first order along the surface of the body [9]. A separate system of fundamental solutions is used to represent the head [10], and the hydrodynamic interactions between the head and the tail are taken into account using Faxén's laws [11]. In the framework of this singularity method, the hydrodynamics is governed by an integral equation for the distribution of forces along the swimmer. The governing equations are solved numerically using a midpoint collocation scheme for which the tail is discretized into a regular grid of N elements (typically $N \approx 100$).

We seek to find periodic beating patterns for our model uniflagellated swimmers, which maximize the swimming efficiency $\mathcal{E}$. These optimal strokes are computed [e.g., using MATLAB'S `fmincon()` routine] subject to the constraint that there is no net rotation of the swimmer after one stroke. A discrete representation for $\gamma(t,s)$ is obtained by imposing the curvature at a finite set N_γ of equidistant nodes of arc length s_{N_γ} along the tail. The number of nodes N_γ was increased incrementally from $N_\gamma = 2$ to 30. At each of these nodes, the curvature $\gamma(t,s_{N_\gamma})$ is a periodic function of time and is represented by the first coefficients of its Fourier decomposition:

$$\Omega_1 = a_0^{\Omega_1} + \sum_{n=0}^{\infty}\left[a_n^{\Omega_1}\cos\left(\frac{2\pi}{\tau}nt\right) + b_n^{\Omega_1}\sin\left(\frac{2\pi}{\tau}nt\right)\right]. \quad (4)$$

Hence, $\mathcal{E}$ is a nonlinear function of the Fourier coefficients parametrizing the kinematics of the stroke. The curvature for all s along the tail can then be deduced by cubic spline interpolation.

Since $\mathcal{E}$ only depends on the stroke kinematics and two dimensionless parameters characterizing the geometry of the swimmer η and κ, we varied the values of the head diameter and tail length from $D = 2$ to 20 μm and $L = 5$ to 200 μm, respectively, and fixed the value of the tail radius $r = 0.150$ μm. To explore the space of all acceptable kinematics, the optimization procedure was started from a wide range of initial strokes, which varied in structure, symmetry, and amplitude. Figure 1(b) represents a small sample of the initial strokes used, including symmetric and asymmetric strokes, small and large amplitudes, traveling waves of growing amplitude, and meandering strokes. The number of initial strokes used was particularly extensive for small values of $N_\gamma \leqslant 5$, for which the reduced number of optimization parameters

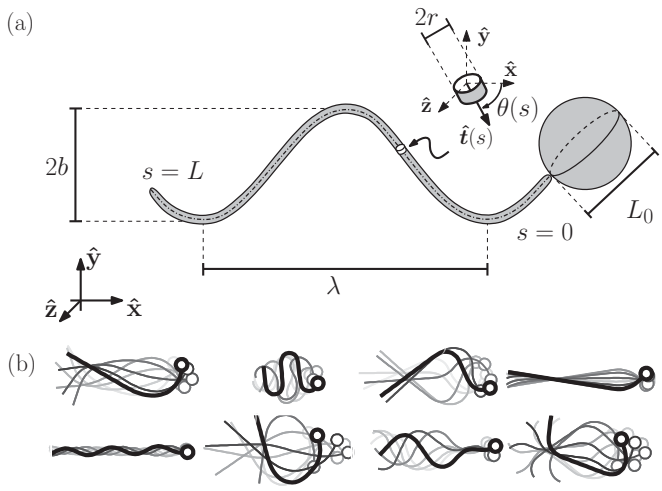

FIG. 1. (a) Model swimmer parameters. (b) A sample of initial guesses used in the optimization procedure. The gray scale schematics indicate snapshots at earlier times.

allowed a systematic sampling of initial strokes. In all cases, the optimization procedure converged to the same solution: symmetrical undulatory bending waves with localized regions of high curvature, which form at the base of the head and propagate toward the end of the flagellum.

A representative optimized swimmer computed with $N_\gamma = 30$ is shown in Fig. 2 with $D = 3$ μm and $L = 36$ μm. Figure 2(a) represents superposed snapshots of the optimal stroke. The undulatory nature exhibited by this optimal stroke is in qualitative agreement with strokes observed in biological uniflagellates swimming in viscous media and in particular with sperm cells of varying dimensions [3,12,13]. The efficiency of this optimal stroke is $\mathcal{E} \approx 1.1\%$, which corresponds to an increase of $\approx 37\%$ over the maximum efficiency of 0.8% attained by the same swimmer using a sinusoidal waveform [5].

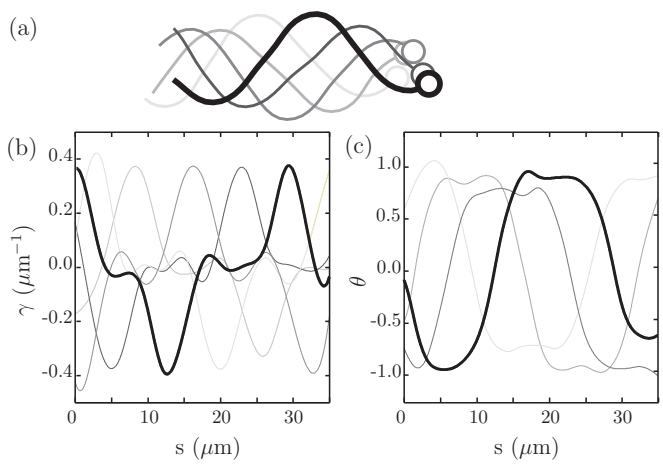

FIG. 2. Optimal swimming stroke. (a) Time series of optimal stroke. (b) Optimal curvature as a function of arc length. (c) Angle between the swimming direction and the (local) angle of the flagellum. Gray-scale images in all three panels indicate snapshots at earlier times.

Figure 2(b) represents the curvature of the optimal stroke $\gamma(s,t)$ along the flagellum. At each time, the curvature $\gamma(s,t)$ remains close to zero at all locations along the tail except for finite regions of high curvature of alternating sign, propagating toward the end of the flagellum. The waveform of the optimized stroke is therefore best described as a rounded sawtooth, for which the flagellum remains mostly straight except for narrow regions concentrating most of the bending deformation. This can also be seen in Fig. 2(c), which shows the angle $\theta(t,s)$ between the swimming direction and the unit vector tangent to the flagellum $\hat{\mathbf{t}}$ as a function of the arc length s. For a sawtooth waveform, $\theta(t,s)$ would be a perfect square wave propagating along the flagellum. In contrast, $\theta(t,s)$ is a rounded square wave for the optimized stroke, corresponding to a rounded sawtooth waveform [see Fig. 2(a)]. This result is in agreement with experimental observations of the waveforms of swimming spermatozoa, which have been described as "circular arcs connected by straight lines" [12,13]. In addition, the ratio between the wave amplitude b and the wavelength λ [see Fig. 1(a)] is found to be $\approx$0.21 for the computed stroke, while it has been measured experimentally for different species to be $\approx$0.20 [12]. Likewise, the number of complete wave periods per tail is $\approx$1.23 for our computed stroke and has been measured experimentally to be $\approx$1.25–1.4 [12].

It should be stressed that our optimization procedure always converged to the same optimal stroke regardless of the initial guess, which suggests a simple structure for the efficiency in the space of possible strokes. This fact—while not being rigorous proof of the uniqueness of the solution—is nevertheless a strong indication that undulatory traveling waves may be among of the most efficient swimming strategies for uniflagellated swimmers at low Reynolds number.

Having computed optimal kinematics for given geometries, we now seek to determine whether hydrodynamics plays a dominant role, not only in stroke selection but also in the evolution of sperm morphology. For a given head size D, corresponding to a given volume of genetic material, we seek optimal values for the geometric parameter $\eta = L/D$. One can argue that such optimal values of η should exist by considering two extreme cases: $L \to 0$ and $L \to \infty$. As the length of the tail approaches zero, the swimmer becomes a single rigid sphere and can no longer propel itself; hence the swimming efficiency is zero. Similarly, as the length of the tail goes to infinity, most of the mechanical power is used to overcome the drag on the (infinitely long) tail, and again the efficiency associated with transport of the head (i.e., the "payload") decays to zero. Between these two extremes there exist strokes with efficiencies greater than zero, therefore at least one optimal value must exist.

To find these optimal morphologies, we selected head diameters $D = 2$–$10\ \mu$m and varied the length of the tail L. For each geometry, we computed the optimal stroke kinematics and the associated swimming efficiency by using our optimization procedure. We found that, for a given head size, optimal values of L exist, consistent with previous work [5], which investigated swimmers using prescribed suboptimal sinusoidal strokes. Values of $\mathcal{E}$ are shown in Fig. 3. Each point in the figure represents a separate optimization calculation of the kinematics for a given geometry D and L. Hence the optimal kinematics for a short tail at the far left in the graph

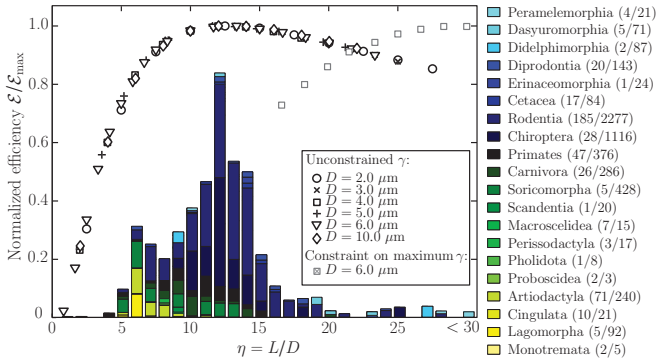

FIG. 3. (Color online) Black symbols: normalized efficiency of the computed optimal strokes as a function of the tail-to-head length ratio $\eta = L/D$ for $D = 2$–$10\ \mu$m and $r = 0.150\ \mu$m, with no constraint imposed on the curvature. Gray symbols: normalized efficiency for swimmers with $D = 6\ \mu$m and $r = 0.5\ \mu$m for which a maximum curvature constraint $1/\gamma > 30\ \mu$m is imposed. Histogram: distribution of mammalian species as a function of the geometric parameter η. Colors correspond to the different orders in the data set. For each order, the first number corresponds to the number of species in our data set, the second to the total number of species in the order.

may be different from those of a longer tail at the far right. Our numerical results collapse onto a single curve when the efficiency is normalized with the maximum efficiency achieved for each value of D and plotted as a function of η (see Fig. 3). Thus the optimal morphology of our model swimmer is fully characterized by a single nondimensional geometric parameter $\eta = L/D$, and maximum efficiencies are obtained at $\eta \approx 12$ (see Fig. 3). The peak in efficiency is broad around the optimum and $\mathcal{E}$ lies within 80% of the maximum efficiency for values of η ranging from $\eta = 5.5$ to 31. The optimal value of $\eta \approx 12$ involves no fitting parameters, no material properties, and stems purely from hydrodynamic considerations, hence we can expect it to be relevant to a broad range of uniflagellated microswimmers.

Previous comparative studies have demonstrated a positive correlation between head and tail sizes [14,15]. To determine the relevance of the optimal criterion, $\eta \approx 12$, to biological microswimmers, we collected data on mammalian sperm morphometry from published sources [14–20]. We found measurements for 440 mammalian species covering 7.9% of known mammalian species and including 20 out of 28 mammalian orders. In general, the anatomy of a spermatozoon can be divided into three sections: the head, the midpiece, and the tail, the midpiece being a region at the base of the flagellum that is thicker than the flagellum itself. Since our model swimmer has a simple two-component head-tail geometry, we considered the tail length to be the sum of the midpiece L_m and tail lengths for all species where measurements of head, midpiece, and tail were available. We found the average value for the ratio η in our data set to be 11.8 ± 4.0, coinciding with the computed optimal morphology, $\eta \approx 12$. For 96% (85%) of all species in our data set, we found that measured values for η allow for swimming within 80% (90%) of the maximal efficiency. Hence, sperm cells of nearly all species in our data set exhibit hydrodynamically efficient morphologies.

Our data set oversamples some mammalian orders, i.e., we collected data on 71 of the 240 species of *Artiodactyla* (even-toed ungulates, such as goats, pigs, etc.) but only 28 of the 1116 species of *Chiroptera* (bats). To correct for oversampling of a given order, the distribution of species in each order is rescaled with the data coverage. Figure 3 represents the distribution of mammalian species with respect to the morphological ratio η. It is noteworthy that, unlike the peak in $\mathcal{E}$ that is broad around the optimum, the peak in the distribution of collected biological data is sharp. The cluster of data surrounding the optimal value of η is striking and suggests a strong selective pressure on the morphology of sperm cells.

While the agreement is particularly remarkable for the largest mammalian orders *Rodentia* (rodents) and *Chiroptera* (bats) (see Fig. 3), it is worth commenting on the outliers in the histogram for which η appears to be suboptimal. The first points of interest are the species with large η ($\geqslant 25$), corresponding to rodents and small marsupial bandicoots. Their tails are unusually long ($L \geqslant 150\ \mu$m) and thick ($r \geqslant 0.5\ \mu$m). The increased tail thickness has been correlated with enhanced tensile strength and resistance to shear stress [21]. Sperm cells with thick tails have been observed to undergo strokes with larger radii of curvature due to the increased bending stiffness of the flagellum [22]. The first-order effects of increasing bending stiffness can be approximated by imposing a minimum radius of curvature γ_0, such that the local curvature $\gamma(s,t) \geqslant \gamma_0$ everywhere. Modified results that include the minimal curvature constraint are represented by the gray symbols in Fig. 3, indicating that, for stiffer tails, the optimal morphology shifts toward larger values of η. This effect, however, is relevant only in very thick tails as the bending stiffness scales $\sim r^4$ and hence decreases sharply with r. At the opposite end of the histogram, the order *Monotremata* (egg-laying mammals) displays a very low tail-to-head length ratio $\eta \leqslant 2$. However, the dimensions and shape of their heads, $\approx 50\ \mu$m long and $\approx 0.7\ \mu$m wide [23], are very far from the spherical head hypothesis of our model, which does not account for variations in head geometry.

Finally, a more puzzling discrepancy is the existence of a second smaller peak at $\eta \approx 6$ in the biological histogram for which there is no corresponding feature in the computed optimal curve. This peculiar second peak is due primarily to the orders *Lagomorpha* (e.g., rabbits and pikas) and *Artiodactyla*. From a hydrodynamical standpoint, there is no obvious rationalization for this shift, which may be attributed to other factors such as variations in the fluid rheology and in individual or collective sperm behavior. These examples highlight the complexity of biological systems and the importance of species-dependent physical, chemical, and environmental constraints in the evolution of sperm dynamics and morphology.

In summary, we have presented a model system relevant to general aspects of sperm motility. For typical uniflagellated swimmers, we found the existence of well-defined optimal stroke kinematics and morphologies. The computed optimal geometry is in agreement with experimental observations of sperm cells across a wide range of mammalian species, and both the existence and the functional form of this correlation can be theoretically rationalized from hydrodynamic considerations.

[1] W. Sutherland, Nature (London) **435**, 569 (2005).
[2] I. Gibbons, J. Cell Biol. **91**, 107 (1981).
[3] G. Hancock, Proc. R. Soc. London, Ser. A **217**, 96 (1953).
[4] O. Pironneau and D. Katz, J. Fluid Mech. **66**, 391 (1974).
[5] J. Higdon, J. Fluid Mech. **90**, 685 (1979).
[6] D. Tam and A. E. Hosoi, Phys. Rev. Lett. **98**, 068105 (2007).
[7] E. Lauga and T. Powers, Rep. Prog. Phys. **72**, 096601 (2009).
[8] S. Suarez and A. Pacey, Hum. Reprod. Update **12**, 23 (2006).
[9] J. Keller and S. Rubinow, J. Fluid Mech. **75**, 705 (1976).
[10] A. Chwang and T. Wu, J. Fluid Mech. **67**, 787 (1975).
[11] J. Happel and H. Brenner, Low Reynolds Number Hydrodynamics (Noordhof, Leyden, 1973).
[12] C. Brokaw, J. Exp. Biol. **43**, 155 (1965).
[13] D. Johnston, N. Silvester, and M. Holwill, J. Exp. Biol. **80**, 299 (1979).
[14] M. Gage, Proc. R. Soc. London, Ser. B **265**, 97 (1998).
[15] J. Cummins and P. Woodall, J. Reprod. Fert. **75**, 153 (1985).
[16] S. Plön and R. Bernard, J. Zool. **269**, 466 (2006).
[17] P. Cetica, I. Rahn, M. Merani, and A. Solari, Biocell **21**, 195 (1997).
[18] P. Cetica, J. Sassaroli, M. Merani, and A. Solari, Biocell **18**(1), 89 (1993).
[19] S. Jeong, J. Park, H. Kim, C. Sik Bae, M. Yoon, D. Lim, and M. Jeong, Biocell **30**, 279 (2006).
[20] M. Anderson, J. Nyholt, and A. Dixson, J. Zool. **267**, 135 (2005).
[21] J. Baltz, P. Williams, and R. Cone, Biol. Reprod. **43**, 485 (1990).
[22] D. Phillips, J. Cell Biol. **53**, 561 (1972).
[23] F. Carrick and R. Hughes, Cell. Tissue Res. **222**, 127 (1982).